

# Adipose mesenchymal stem cell-derived extracellular vesicles reduce glutamate-induced excitotoxicity in the retina

Tian-Qi Duan<sup>1</sup>, Zhao-Lin Gao<sup>1</sup>, Ai-Xiang Luo<sup>1</sup>, Dan Chen<sup>1</sup>, Jian-Bin Tong<sup>2</sup>, Ju-Fang Huang<sup>1,\*</sup>

<https://doi.org/10.4103/1673-5374.369123>

Date of submission: September 26, 2022

Date of decision: December 14, 2022

Date of acceptance: January 20, 2023

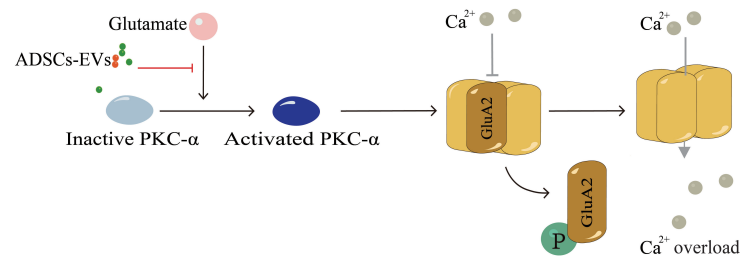
Date of web publication: March 3, 2023

## From the Contents

Introduction	2315
Methods	2316
Results	2317
Discussion	2319

## Graphical Abstract

*Extracellular vesicles of adipose mesenchymal stem cells (ADSCs-EVs) attenuate retinal excitotoxicity by regulating the phosphorylation of GluA2*



## Abstract

Adipose mesenchymal stem cells (ADSCs) have protective effects against glutamate-induced excitotoxicity, but ADSCs are limited in use for treatment of optic nerve injury. Studies have shown that the extracellular vesicles (EVs) secreted by ADSCs (ADSC-EVs) not only have the function of ADSCs, but also have unique advantages including non-immunogenicity, low probability of abnormal growth, and easy access to target cells. In the present study, we showed that intravitreal injection of ADSC-EVs substantially reduced glutamate-induced damage to retinal morphology and electroretinography. In addition, R28 cell pretreatment with ADSC-EVs before injury inhibited glutamate-induced overload of intracellular calcium, downregulation of  $\alpha$ -amino-3-hydroxy-5-methyl-4-isoxazolepropionic acid receptor (AMPA) subunit GluA2, and phosphorylation of GluA2 and protein kinase C alpha *in vitro*. A protein kinase C alpha agonist, 12-O-tetradecanoylphorbol 13-acetate, inhibited the neuroprotective effects of ADSC-EVs on glutamate-induced R28 cells. These findings suggest that ADSC-EVs ameliorate glutamate-induced excitotoxicity in the retina through inhibiting protein kinase C alpha activation.

**Key Words:** adipose mesenchymal stem cells; calcium overload; electroretinography; excitotoxicity; extracellular vesicles; GluA2; glutamate; protein kinase C alpha; R28 cells; retina; retinal ganglion cell

## Introduction

Excitotoxicity is now recognized as a crucial pathophysiological mechanism in a multitude of retinal diseases, including glaucoma (Vernazza et al., 2021), diabetic retinopathy (Zaitone et al., 2020; Alomar et al., 2021), and retinal vein occlusion (Wasilewa et al., 1976; Dionysopoulou et al., 2020). Memantine, an N-methyl-D-aspartic acid receptor (NMDAR) inhibitor, is the primary strategy for alleviating excitotoxicity in the clinic (Liu et al., 2020). However, oral memantine may result in side effects, including wooziness, headaches, constipation, and diarrhea (Kuns et al., 2022). Therefore, the clinical anti-excitotoxic treatment of retinal diseases remains an important issue (Chen and Kukley, 2020).

In recent years, mesenchymal stem cell (MSC)-based cell transplantation therapy has become a promising approach for treating retinal disorders. This therapeutic strategy is attributed to the ability of MSCs to transdifferentiate into neurons, their self-renewal abilities, pro-proliferative properties, and neuroprotective effects (Harrell et al., 2019, 2022). Previous studies have identified a protective role for adipose mesenchymal stem cells (ADSCs) in glutamate-induced excitotoxic injury, but the mechanism is not clear (Zhao et al., 2009; Hao et al., 2014). Further, there are still some limitations of MSC therapy in the eye, including few cells integrated into the retina, abnormal growth, and immune rejection (Yu et al., 2020). It has been found

that intravitreal injection of MSC-derived extracellular vesicles (EVs) reduces apoptosis of retinal ganglion cells (RGCs) in a rat model of acute intraocular hypertension (Mathew et al., 2019). Thus, it may be possible to avoid the limitations of ADSCs by using EVs in the treatment of retinal diseases.

Excessive activation of ion-associated glutamate receptors is critical in the pathogenesis of glutamate-induced retinal damage (Connaughton, 1995; Xu et al., 2017). Ion-associated glutamate receptors include NMDARs, kainate receptors, and  $\alpha$ -amino-3-hydroxy-5-methyl-4-isoxazolepropionic acid receptors (AMPA) (Dingledine et al., 1999). In contrast to NMDARs, AMPARs are almost impermeable to calcium ions under physiological conditions (Bowie and Mayer, 1995; Jacobi and von Engelhardt, 2017). AMPARs are tetrameric membrane proteins consisting of four different subunits, GluA1–4. Of all the subunit combinations, the GluA2-lacking AMPARs are permeable to calcium ions (Cull-Candy and Farrant, 2021). Furthermore, an increased expression of GluA2-lacking AMPARs was found in rat models of retinal disease (Dong et al., 2015). It has been reported that the GluA2 deletion mechanism is associated with GluA2 phosphorylation (S880). Additionally, activation of the protein kinase C (PKC) pathway may be a key GluA2 stimulator (Purkey and Dell'Acqua, 2020; Guo and Ma, 2021). Hence, upregulating GluA2 expression and inhibiting its phosphorylation may be a reliable approach to ameliorate glutamate-induced retinal damage.

<sup>1</sup>Department of Anatomy and Neurobiology, School of Basic Medical Sciences, Central South University, Changsha, Hunan Province, China; <sup>2</sup>Hunan Province Key Laboratory of Brain Homeostasis, Third Xiangya Hospital, Central South University, Changsha, Hunan Province, China

\*Correspondence to: Ju-Fang Huang, PhD, [huangjufang@csu.edu.cn](mailto:huangjufang@csu.edu.cn).

<https://orcid.org/0000-0002-9161-1055> (Ju-Fang Huang); <https://orcid.org/0000-0001-6654-8114> (Tian-Qi Duan)

**Funding:** This study was supported by the National Key R&D Program of China, No. 2016YFC1201800 (to JFH); the Key Research and Development Program of Hunan Province, Nos. 2018SK2090 (to JFH), 2022SK2079 (to JFH); the Natural Science Foundation of Hunan Province, No. 2021JJ30891 (to DC); the Human Resource Bank Program of Hunan Province, No. 2020TP3003 (to JFH); and the School-Enterprise Joint Program of Central South University, No. 2021XQLH092 (to TQD).

**How to cite this article:** Duan TQ, Gao ZL, Luo AX, Chen D, Tong JB, Huang JF (2023) Adipose mesenchymal stem cell-derived extracellular vesicles reduce glutamate-induced excitotoxicity in the retina. *Neural Regen Res* 18(10):2315-2320.

In the present study, we investigated whether ADSC-EVs inhibit glutamate-induced retinal excitotoxic damage *in vivo* and *in vitro*, and their effects on GluA2 and PKC.

## Methods

### Ethics statement

All adipose tissue collections were approved by the Medical Ethics Committee of Central South University (IRB No. 202111001) on November 9, 2021, and all volunteers signed informed consent. All animal experiments were approved by the Animal Ethics Committee of Central South University (No. CSU-2022-0088) on February 22, 2022. All animal experiments were reported according to the Animal Research: Reporting of *In Vivo* Experiments (ARRIVE) guidelines (Percie du Sert et al., 2020).

### Experimental design

#### *In vivo* experiments

In total, 38 specific-pathogen-free male Sprague-Dawley rats, weighing 200 g and aged 6–8 weeks, were purchased from the Hunan SJA Laboratory Animal Co., Ltd. (Changsha, Hunan, China) (license No. SYXK (Xiang) 2020-0019). The animals were housed in a specific-pathogen-free environment, under a 12-hour light/dark cycle, 60 ± 5% humidity, and a temperature of 23 ± 1°C. They were randomly divided into six groups with the following treatments: Con group: intravitreal injection of 4 µL phosphate buffered saline (PBS) (*n* = 8); Glu group: intravitreal injection of 4 µL 100 mM glutamate (Aladdin, Shanghai, China) (*n* = 8); Glu + EVs group: intravitreal injection of 3 µL of 1 × 10<sup>9</sup> particles/mL ADSC-EVs, followed by intravitreal injection of 4 µL of 100 mM glutamate 1 hour later (*n* = 8); Glu + PBS group: intravitreal injection of 3 µL PBS, followed by intravitreal injection of 4 µL of 100 mM glutamate 1 hour later (*n* = 8); PKH26-Control group: intravitreal injection of 3 µL PBS (*n* = 3); and PKH26-labeled group: intravitreal injection of 3 µL of 1 × 10<sup>9</sup> particles/mL PKH26-labeled ADSC-EVs (*n* = 3). Intravitreal injection was performed by inserting the needle 1 mm outside the limbus using a micro syringe (Hamilton, Reno, NV, USA) after the pupil was dilated with compound tropicamide (Bausch & Lomb, Jinan, Shandong, China). Animals were killed 24 hours after intravitreal injection (Sisk and Kuwabara, 1985) (**Figure 1**).

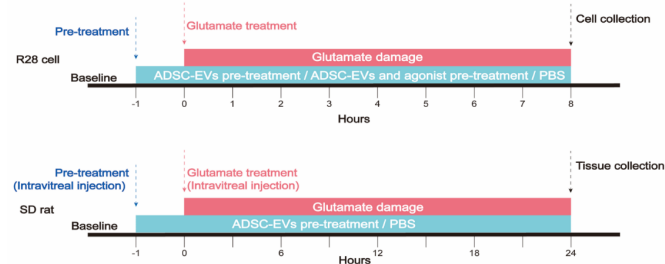


**Figure 1 | Schematic of the experimental timeline of *in vitro* and *in vivo* modeling.**

In the *in vitro* model (top panel), R28 cells were pretreated with ADSC-EVs (or PBS for control) or ADSC-EVs and agonists for 1 hour before establishing the glutamate induction model. The control group was kept under normal culture conditions for the same length of time (8 hours). In the *in vivo* model (bottom panel), ADSC-EVs (or PBS for control) were injected into the vitreous cavity 1 hour before glutamate intravitreal injection. In the control group, the same volume of PBS (4 µL) was injected intravitreally into the vitreous cavity for the same length of time (24 hours). ADSC-EVs: Adipose mesenchymal stem cell-extracellular vesicles; PBS: phosphate buffered solution; R28: rat retinal precursor vesicles; SD: Sprague-Dawley.

### *In vitro* experiments

Rat retinal precursor (R28) cells were provided by Central South University. This cell line had been characterized by short tandem repeat analysis and confirmed according to the ICLAC Database of Cross-Contaminated or Misidentified Cell Lines. In previous studies (Lee et al., 2020; Huang et al., 2021; Yao et al., 2022; Yan et al., 2023), the R28 cell line has been widely used to explore the neuroprotection and pathological mechanism of RGCs *in vitro*. To determine the optimal time point for glutamate damage on R28 cells, we treated cells with 34 mM glutamate for 4, 6, 8, 10, and 12 hours. To determine the most effective concentration of ADSC-EVs to protect R28 cells, we pretreated cells with 5 or 25 µg/mL ADSC-EVs for 1 hour. We pretreated cells with 10, 25, 50, 75, and 100 ng/mL 12-O-tetradecanoylphorbol 13-acetate (TPA; Beyotime, Shanghai, China) for 1 hour to determine the optimal concentration of TPA, which activates the PKC pathway. *In vitro* experiments included in five groups with the following treatments: Con group: cells were cultured under normal conditions; Glu group: cells were treated with 34 mM glutamate; Glu + EVs group: cells were pretreated with ADSC-EVs for 1 hour before the addition of glutamate; Glu + PBS group: cells were pretreated with PBS before the addition of glutamate; and Glu + TPA + EVs group: cells were pretreated with TPA and ADSC-EVs for 1 hour before the addition of glutamate. We cultured the cells at least three times, and three dishes were used for each group during each culture (**Figure 1**).

### Culture and identification of ADSCs

Human-derived ADSCs were isolated and cultured using the methods described in a previous study (Ahmadian Kia et al., 2011). Briefly, adipose

tissue of healthy adults aged 18–50 years old collected from the Third Xiangya Hospital of Central South University was mechanically chopped before centrifugation at 450 × *g* for 5 minutes. Afterward, we collected the middle layer of the three-layer fraction, which is the stromal vascular fraction (Hearnden et al., 2021). Then the stromal vascular fraction was digested with 0.1% collagenase I (Servicebio, Wuhan, China; GC305013) in a 37°C incubator with 225 r/min shaking for 30–60 minutes. We filtered the digested tissue solution with a 40-µm filter and centrifuged it at 450 × *g* for 10 minutes. The pellet was resuspended in a low glucose Dulbecco's modified Eagle's medium (Hyclone, Logan, UT, USA; Cytiva SH30021.01) containing 10% fetal bovine serum (ExCell Bio, Suzhou, China). The cells were stored in a sterile moist environment of 37°C and 5% carbon dioxide. After reaching 80–100% confluence, we passaged the cells with 0.25% trypsin (Gibco, Grand Island, NY, USA).

After the third generation of cell transmission, we identified the characteristics and differentiation ability of the cells. Initially, cell morphology was observed by light microscopy, and then cells were digested with trypsin (Gibco), resuspended in culture medium, and transported at 4°C for flow cytometry (Changsha Golden Medical Clinical Laboratory Center, Changsha, China). In addition, we also performed lipogenic and osteogenic differentiation assays on ADSCs (Cyagen Biosciences, Santa Clara, CA, USA; HUXMD-90031, HUXMD-90021). Briefly, we first inoculated the cells in a 6-well plate coated with 1% gelatin, and when the cell fusion reached 70%, 2 mL of the prepared medium for differentiation induction was added to the wells. After 2–4 weeks, the cells were stained with Alizarin Red and Oil Red O (Cyagen Biosciences) to observe the morphological changes and growth.

### Extraction and identification of ADSC-EVs

In accordance with previous methods (Dou et al., 2020; Yang et al., 2020), we obtained EVs by ultrafiltration combined with a polymer precipitation strategy. Briefly, cells were cultured for more than 48 hours in a serum-free medium (Hyclone; Cytiva SH30021.01). Then we removed cells and debris by centrifugation (200 × *g*, 10 minutes, 4°C). The supernatant was concentrated using a 0.45-µm filter and a 100-kDa ultrafiltration tube (Millipore, Burlington, MA, USA; UFC9100, Amicon Ultra-15). Thereafter, EVs were pelleted by low-speed centrifugation (1500–3000 × *g*) after overnight incubation with polyethylene glycol at 4°C. Then, precipitates were resuspended in sterile PBS and EVs were obtained for further applications. Finally, we performed nanoparticle tracking analysis (Particle Metrix, Munich, Germany; ZetaView), electron microscopy, and western blot to identify the concentration, size, shape, and surface markers of ADSC-EVs.

### ADSC-EVs uptake by rat retina and R28 cells

EVs were labeled according to the instructions of the PKH26 Red Fluorescent Cell Ligation Kit (Umibio, Shanghai, China; UR52302). Briefly, EVs were suspended in 10 µL diluted PKH26 solution (1 µL PKH26 and 9 µL PBS) for 10 minutes. After that, we washed the mixture in 10 mL 1× PBS and concentrated it in a 100-kDa ultrafiltration tube (3000 × *g*, 20 minutes, 4°C). The pellets were resuspended and added to the R28 cells at 25 µg/mL. After incubating with PKH-labeled EVs for 8 hours, the cells were stained with 4',6-diamidino-2-phenylindole (DAPI, Solarbio, Beijing, China) and observed by fluorescence microscope (Zeiss, Jena, Germany, AXIO Vert.A1).

For the *in vivo* experiments, 24 hours after the intravitreal injection of 3 µL 1 × 10<sup>9</sup> particles/mL PKH26-labeled EVs, the rats were anesthetized with an intraperitoneal injection of 2% sodium pentobarbital (40 mg/kg; FWD Chemical Company, Shanghai, China) and perfused with 4% paraformaldehyde via myocardium. Then, the eyeballs were removed and fixed in ocular fixative (Servicebio, G1109) for more than 1 day, dehydrated in 30% sucrose, embedded with optimal cutting temperature compound (Sakura, Tokyo, Japan; 4583), and then stored at –80°C. The eyeballs were sectioned sagittally with a cryostat (Leica, CM1520) at a thickness of 8 µm. After DAPI staining, the sections were observed using a fluorescence microscope.

### Hematoxylin and eosin staining

After 2% sodium pentobarbital anesthesia and 4% paraformaldehyde cardiac perfusion as above, bilateral eyeballs were removed with forceps and then fixed in an ocular fixative for more than 1 day. Subsequently, we embedded the eyeballs in paraffin and then obtained continuous sagittal sections (4 µm thick), including the optic nerve head. After staining with hematoxylin and eosin (Servicebio, G1003), we observed the morphology of retinal layers using a light microscope (Toupcam, Hangzhou, China) analyzed by ImageJ software and Adobe Illustrator 26.0 (San Jose, CA, USA) software. The number of RGCs, and thickness of the inner plexiform layer and inner nuclear layer in one paraffin section per eye were recorded at 1000-µm intervals beginning at the optic papilla.

### Electroretinography

Electroretinography (ERG) waveforms were recorded 24 hours after modeling by an eye electrophysiological detector (Roland, Brandenburg, Germany; RETI port/scan 21). Before dark-adapted ERG assays, rats were maintained in a dark environment for 24 hours. After anesthetization with 1% sodium pentobarbital (50 mg/kg), ERG data were collected by full field stimulation. The original data of scotopic 3.0 and 3.0 cd s/m<sup>2</sup> oscillatory potential ERG were recorded and analyzed by Microsoft Excel 2016 (Redmond, WA, USA) software. Next, we measured the a-wave amplitude from the prestimulated baseline to the wave trough. The b-wave amplitude was measured from the trough of the a-wave to the peak of the waveform. The analysis and description of the scotopic 3.0 oscillatory potentials (SOPs) were mainly based

on the peaks of the three main oscillatory waveforms in the signal (McCulloch et al., 2015).

**Propidium iodide staining**

Propidium iodide (PI) staining is regarded as a marker of necrotic cells (Crowley et al., 2016). After washing twice with PBS, the R28 cells were incubated in PI-dye solution (10 µg/mL; Sigma, St. Louis, MO, USA, Cat# P4170) for 15 minutes. Subsequently, the cells were fixed with 4% paraformaldehyde for 20 minutes and nuclei were stained with DAPI for 5 minutes. Finally, the ratio of necrotic cells was calculated as PI-positive cells/DAPI-positive cells under a microscope.

**Calcium measurement**

After washing three times with calcium-free Hank's balanced salt solution (Solarbio), the cells were labeled by 4 µM fluorescent probe (Fluo-4 AM, Solarbio) for 30 minutes at 37°C. Then, the cells were fixed with 4% paraformaldehyde and stained with DAPI. The Fluo-4 AM signal was observed using a fluorescence microscope. The fluorescence signal intensity values of Fluo-4 AM were obtained by dividing the integrated density by the number of cells, as described in a previous study (Wang et al., 2019). ImageJ v.1.5.1 (National Institutes of Health, Baltimore, MD, USA) software (Schneider et al., 2012) was used for integrated density measurement and cell counting.

**Western blot analysis**

The R28 cells were lysed for 30 minutes in radioimmunoprecipitation assay lysis buffer (CWBI0, Beijing, China) with the addition of protease and phosphatase inhibitors (Roche, Basel, Switzerland). After performing electrophoresis and electroblotting, we blocked the nitrocellulose membranes (Pall, New York, NY, USA, Cat# 66485) in 5% nonfat milk (MengNiu, Hohhot, Inner Mongolia, China) or QuickBlock™ Blocking Buffer (Beyotime, P0252) at room temperature (approximately 25°C) for 1–2 hours. The samples were incubated with the following primary antibodies overnight at 4°C: 1) Extracellular vesicles and MSC surface markers: polyclonal rabbit anti-CD81 (1:1000; GeneTex, Irvine, CA, USA, Cat# GTX101766, RRID: AB\_10618892) and anti-CD63 (1:1000; Wanleibio, Shenyang, Liaoning Province, China, Cat# WL02549, RRID: AB\_2910631); 2) Key regulatory proteins of AMPAR: polyclonal rabbit anti-GluA2 (1:1000; Abclonal, Wuhan, China, Cat# A0111; RRID: AB\_2756954), polyclonal rabbit anti-phospho-GluA2 (Ser 880; 1:500; Affinity Bioscience, Beijing, China, Cat# AF3307, RRID: AB\_2834726), polyclonal rabbit anti-PKC alpha (1:1000; Wanleibio, Cat# WL02234, RRID: AB\_2925211), and monoclonal rabbit anti-phospho-PKC alpha (1:10,000; Abcam, Cambridge, UK, Cat# ab32502, RRID: AB\_777295); 3) Apoptosis-related proteins: polyclonal rabbit anti-cleaved caspase 3 (1:1000; Cell Signaling Technology, Danvers, MA, USA, Cat# 9661, RRID: AB\_2341188); and monoclonal rabbit anti-β-tubulin (1:10,000; Proteintech, Wuhan, China, Cat# 66240-1-Ig, RRID: AB\_2881629). After washing in PBS-Tween 20 (0.05%), the membranes were incubated with goat anti-rabbit IgG (1:10,000; Abbkine, Wuhan, China, Cat# A25222, RRID: AB\_2922982) at room temperature for 2 hours. The immunoreactive band was then visualized using a high sensitivity chemiluminescent reagent (CWBI0). The grayscale intensities quantified with ImageJ software were normalized to the control and β-tubulin.

**Immunofluorescence staining**

R28 cells were fixed for 20 minutes with 4% paraformaldehyde. Then, the cells were washed three times with 0.01 M PBS. The cells were blocked for 1 hour in 5% bovine serum albumin, according to a previous study (Dong et al., 2015). Then, R28 cells were incubated with polyclonal rabbit anti-GluA2 (1:50; Abclonal, Cat# A0111, RRID: WX924262) overnight at 4°C and Alexa Fluor 594-labeled goat anti-rabbit IgG (1:200; Abcam, Cat# ab150160, RRID: AB\_2756445) for 2 hours at room temperature. After staining with DAPI for 5 minutes, images were acquired with a laser-scanning microscope and analyzed by ImageJ software.

**Statistical analysis**

No statistical methods were used to predetermine sample sizes; however, our sample sizes were similar to those reported in previous publications (Charles-Messance et al., 2020; Fang et al., 2023). No animals or data points were excluded from the analysis. All numerical data were recorded by at least two researchers and were analyzed via one-way analysis of variance followed by Brown-Forsythe test using SPSS 22.0 statistical software (IBM, Armonk, NY, USA).  $P < 0.05$  was set as the significance threshold. GraphPad Prism 5 software (GraphPad Software, San Diego, CA, USA, www.graphpad.com) was used to create the bar graphs.

**Results**

**Identification of ADSCs and ADSC-EVs**

ADSCs are characterized by adherent growth, the positive expression of CD105, CD73, and CD90, the negative expression of CD45, CD34, and CD19, and adipogenic and osteogenic abilities (Dominici et al., 2006). We used primary ADSCs from human adipose tissue, and found that 3<sup>rd</sup> generation ADSCs presented a spindle-shaped morphology (Figure 2A). More than 95% of cells expressed the positive markers (CD73, CD105, and CD90), and less than 5% of cells expressed the negative markers (CD34, CD45, and CD19) (Figure 2D). The cells had adipogenic and osteogenic abilities (Figure 2B and C). In addition, EVs were enriched from the medium supernatant of ADSCs. These EVs had a cup shape, with a size distribution peak at 136.87 ± 4.52 nm, and were positive for surface markers CD81 and CD63 (Figure 2E–G), consistent with the characteristics of exosomes (Phinney and Pittenger, 2017). These results confirmed the successful isolation of ADSCs and their EVs.

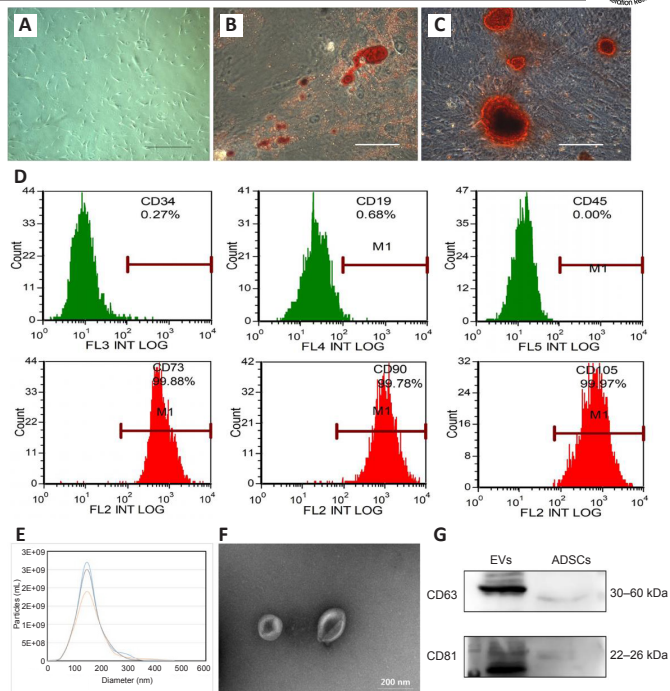


**Figure 2 | Identification of ADSCs and ADSC-EVs.**

(A) Morphology of ADSCs was a spindle shape. (B, C) After induced differentiation, lipid droplets (stained by oil red O) and calcium nodules (stained by Alizarin red) were present in cells. (D) Surface markers of ADSCs were analyzed by flow cytometry. (E) Particle size distribution measured by NTA. (F) Morphologic observation of the EVs under electron microscopy. The EVs had a cup shape appearance. Scale bars: 200 µm (A, F) and 100 µm (B, C). (G) Protein expression of the surface markers CD63 and CD80 on EVs and ADSCs was detected by western blot analysis. ADSCs: Adipose mesenchymal stem cell; EVs: extracellular vesicles; NTA: nanoparticle tracking analysis; PKH-26: red PKH membrane dye.

**ADSC-EVs ameliorate the glutamate-induced damage of the rat retina**

To test the effects of ADSC-EVs on glutamate-induced retinal damage, we injected ADSC-EVs and glutamate into the vitreous sequentially with a 1-hour interval. We found that PKH-26-labeled ADSC-EVs were primarily distributed in RGCs (Figure 3A). Compared with those in the Con group, the number of RGCs ( $P < 0.001$ ; Figure 3B and C), inner plexiform layer thickness ( $P < 0.001$ , Figure 3B and D), inner nuclear layer thickness ( $P < 0.001$ ; Figure 3B and E), and the amplitudes of the a- ( $P < 0.001$ ), b- ( $P < 0.001$ ), and SOP-waves ( $P < 0.001$ ; Figure 3F–J) in ERG were decreased significantly in the Glu group; these alterations were markedly ameliorated in the Glu + EVs group. These findings suggest that ADSC-EVs decreased glutamate-induced inner retinal damage.

**ADSC-EVs reduce intracellular calcium concentration and GluA2 expression in the glutamate damage model**

Increased intracellular calcium concentration plays a vital role in glutamate damage (Hartwick et al., 2008). To assess the effects of ADSC-EVs on the elevated intracellular calcium concentration, R28 cells were treated with EVs for 1 hour before the glutamate supplement. PKH-26-labeled ADSC-EVs were distributed mostly in the cytoplasm of R28 cells (Figure 4A). After application of 34 mM glutamate for 8 hours, more than 50% of R28 cells were necrotic ( $P < 0.001$ ; Additional Figure 1A and B) and intracellular calcium concentration was increased ( $P < 0.001$ ) compared with control group; these changes were considerably ameliorated in the Glu + EVs group (Additional Figure 1C–F and Figure 4B and C).

Additionally, we observed the effect of ADSC-EVs on AMPAR subunit GluA2 expression and phosphorylation in the *in vitro* model of glutamate damage. Compared with the Con group, glutamate damage led to decreased surface GluA2 expression (Figure 4D) and increased GluA2 phosphorylation in R28 cells ( $P < 0.001$ ; Figure 4E and F); the changes were significantly ameliorated in ADSC-EV-treated R28 cells ( $P < 0.001$ ; Figure 4D–F) compared with Glu group. The results suggested that ADSC-EVs reduced the intracellular calcium concentration, upregulated GluA2 expression, and inhibited GluA2 phosphorylation in the *in vitro* glutamate damage model.

**PKC-α activation reduces the effects of ADSC-EVs on GluA2 phosphorylation in glutamate-treated R28 cells**

Previous research has indicated that PKC-α plays a crucial role in regulating GluA2 phosphorylation (Kou et al., 2019). To investigate the mechanism by which ADSC-EVs regulate GluA2 phosphorylation, we activated PKC-α with PKC agonist TPA (100 ng/mL, 1 hour) in R28 cells (Figure 5A and B). ADSC-EVs inhibited the phosphorylation of PKC-α and GluA2 in the Glu + EVs group compared with Glu group (both  $P < 0.001$ ); these changes were significantly reversed in the Glu + TPA + EVs group compared with Glu+EVs group (PKC-α:  $P < 0.01$ , GluA2:  $P < 0.001$ ; Figure 5C–E). The results indicated that ADSC-EVs inhibited PKC-α activation and modulated GluA2 phosphorylation.

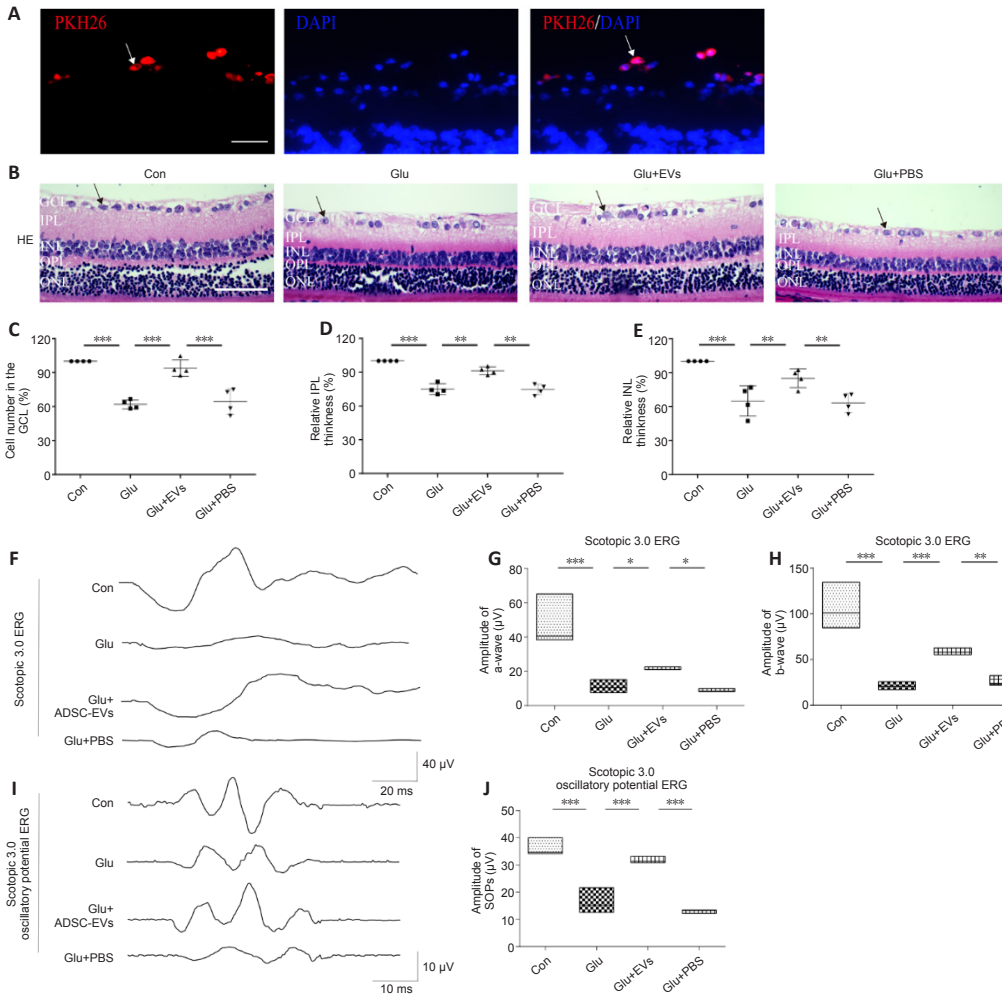


**Figure 3 | ADSC-EVs reduce glutamate-induced morphological and functional damage in rat retina.**

(A) The PKH-26-labeled exosomes (white arrows) in retinas were observed using a fluorescence microscope. (B–E) Representative images and quantitative analysis of hematoxylin and eosin (HE) staining in the retina (mean ± SD,  $n = 4$  rats per group). RGC number, IPL thickness, and INL thickness were decreased significantly in the Glu group; the alterations were markedly improved in Glu + EVs group. The black arrows indicate RGCs. Scale bars: 10 µm (A), 50 µm (B). (F) Representative a- and b-waves under different conditions. The a- and b-wave amplitudes were significantly decreased in the Glu group, and were markedly improved in the Glu + EVs group. (G, H) Statistical analysis of the a- and b-wave amplitudes. (I) Representative sum OPs in scotopic oscillatory potential ERG 3.0 under different conditions. The SOP-wave amplitudes were significantly decreased in the Glu group, and were markedly improved in the Glu + EVs group. (J) Statistical analysis of the SOP-wave amplitudes (mean ± SD,  $n = 4$  rats per group). \* $P < 0.05$ , \*\* $P < 0.01$ , \*\*\* $P < 0.001$  (one-way analysis of variance followed by Brown-Forsythe test).

Con: Intravitreal injection of PBS; Glu: intravitreal injection of glutamate; Glu + EVs: intravitreal injection of ADSC-EVs before the glutamate damage; ADSC-EVs: Adipose mesenchymal stem cells derived extracellular vesicles; DAPI: 4',6-diamidino-2-phenylindole; ERG: electroretinogram; GCL: ganglion cell layer; INL: inner nuclear layer; IPL: inner plexiform layer; ONL: outer nuclear layer; OP: oscillatory potential; PBS: phosphate buffered solution; RGC: retinal ganglion cell; SOP: scotopic 3.0 oscillatory potential.

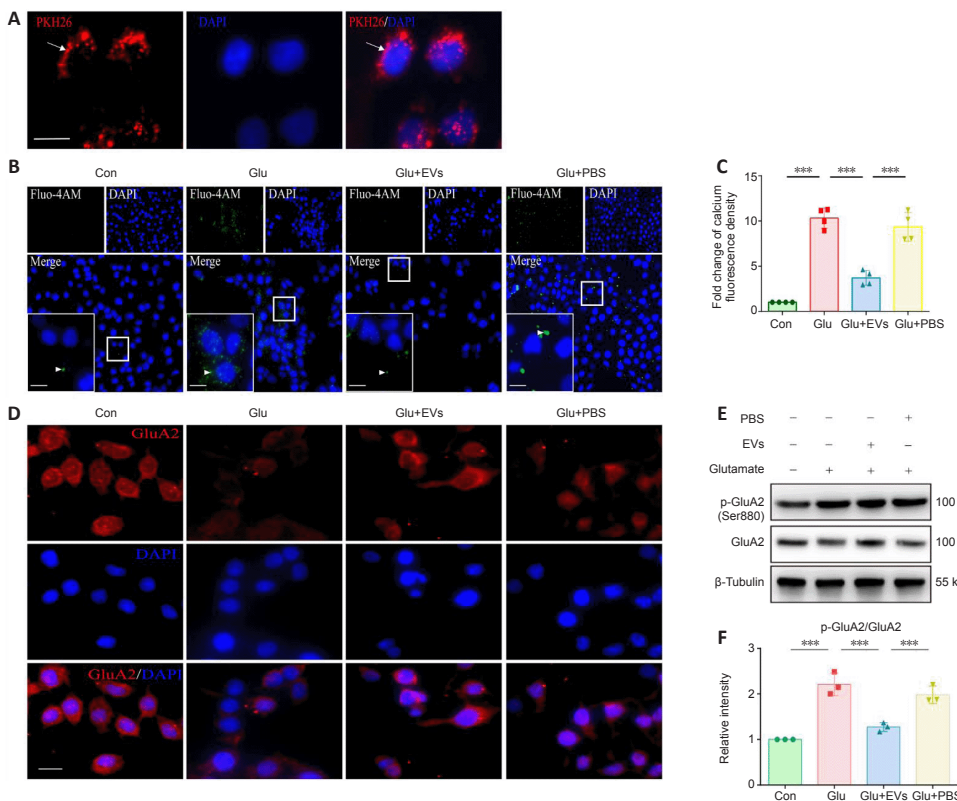


**Figure 4 | ADSC-EVs reduce intracellular calcium concentration by regulating GluA2 expression *in vitro*.**

(A) The PKH-26-labeled exosomes (red, marked with white arrows) in R28 cells. (B) Concentration of calcium ions (white triangles), represented by Fluo-4 signal (green); nuclei stained with DAPI (blue). Glutamate increased the intracellular calcium concentration, which was considerably ameliorated in the Glu + EVs group. (C) Quantitative analysis of Fluo-4 AM fluorescence signal intensity. (D) Immunofluorescent labeling of GluA2 (Alexa Fluor 594, red) on the cell membrane; nuclei stained with DAPI (blue). The surface GluA2 expression in the Glu group was decreased, which was significantly ameliorated in the Glu + EVs group. Scale bars: 10 µm (A, B), 20 µm (D). (E) Western blot of p-GluA2 and GluA2 in R28 cells after treatment with glutamate and ADSC-EVs. (F) The average ratio of p-GluA2/GluA2. Data presented as mean ± SD. \*\*\* $P < 0.001$  (one-way analysis of variance followed by Brown-Forsythe test). Con: R28 cells treated with nothing to add; Glu: R28 cells treated with glutamate; Glu + EVs: R28 cells pre-treated with ADSC-EVs before the glutamate damage; Glu + PBS: R28 cells pre-treated with PBS before the glutamate damage. ADSC-EVs: Adipose mesenchymal stem cell-extracellular vesicles; DAPI: 4',6-diamidino-2-phenylindole; p-GluA2: phospho-GluA2; PBS: phosphate buffered solution; R28: rat retinal precursor cells.

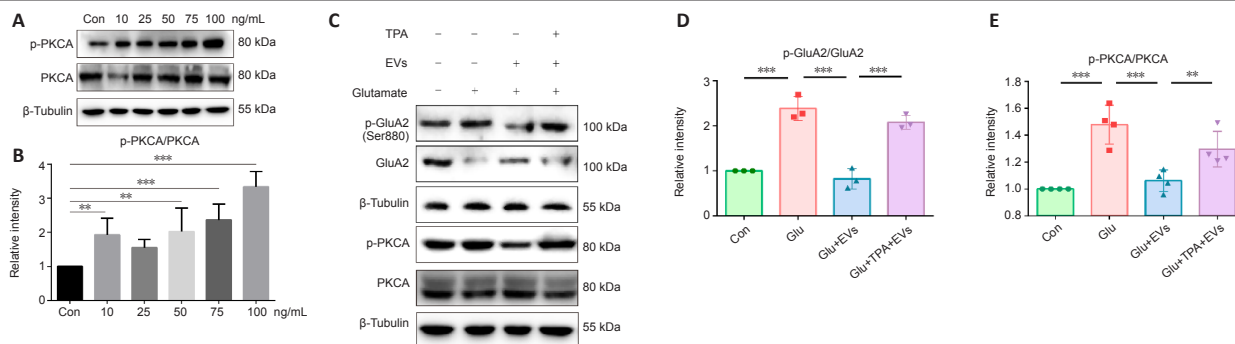


**Figure 5 | PKC- $\alpha$  activation reduces the effects of ADSC-EVs on GluA2 phosphorylation in glutamate-treated R28 cells.** (A) Western blot of p-PKC- $\alpha$  and PKC- $\alpha$  at different TPA concentrations. (B) The bar chart represents the average ratios of p-PKC- $\alpha$ /PKC- $\alpha$ . (C) Western blot of p-GluA2, GluA2, p-PKC- $\alpha$ , and PKC- $\alpha$  in R28 cells after treatment with glutamate, ADSC-EVs, and TPA. (D, E) The bar chart represents the average ratios of p-GluA2/GluA2 and p-PKC- $\alpha$ /PKC- $\alpha$ . Data are presented as mean  $\pm$  SD.  $^{**}P < 0.01$ ,  $^{***}P < 0.001$  (one-way analysis of variance followed by Brown-Forsythe test). Con: R28 cells treated with nothing to add; Glu: R28 cells treated with glutamate; Glu + EVs: R28 cells pre-treated with ADSC-EVs before the glutamate damage; Glu + TPA + EVs: R28 cells pre-treated with TPA before the ADSC-EVs treatment and glutamate damage. ADSC-EVs: Adipose mesenchymal stem cells-extracellular vesicles; p-GluA2: phospho-GluA2; p-PKC- $\alpha$ : phospho-protein kinase C alpha; PKC- $\alpha$ : protein kinase C alpha; R28: rat retinal precursor cells; TPA: 12-O-tetradecanoylphorbol 13-acetate.

## Discussion

Excitotoxicity, a common secondary injury after retinal disease, is significantly associated with the prognosis of retinal structure and function (Dionysopoulou et al., 2020; Vernazza et al., 2021). Our study aimed to explore whether intravitreal injection of ADSC-EVs decreased glutamate-induced retinal damage. The results indicated that intravitreal-injected ADSC-EVs were taken up by RGCs within 24 hours, and the glutamate-induced morphological and functional abnormalities in the inner retinal layers were significantly ameliorated. This is consistent with previous studies (Papazian et al., 2018; Zhuang et al., 2022) on the effects of MSC transplantation on excitotoxicity in a rat controlled cortical impact-induced TBI model and an NMDA-induced mouse cortical neuron damage model. A recent review indicated that intravitreal injection of MSCs in ocular diseases may result in undesirable differentiation and proliferative vitreoretinopathy (Yu et al., 2020). These side effects were not observed in our study. These findings suggest that, as an alternative to stem cell therapy, intravitreal injection of ADSC-EVs is a simple and effective intervention for ameliorating retinal excitotoxicity.

Previous studies have shown that MSC-EVs carry various bioactive cargos such as proteins, microRNAs, lipids, and mRNAs (Bang and Thum, 2012). When MSC-EVs are taken up by targeted cells, these components modulate targeted cells through a variety of pathways. The reported effects include NLRP3 inflammasome inhibition (Zhang et al., 2022), regulation of microglial polarization (Xin et al., 2020), anti-apoptosis (Cui et al., 2022), and promotion of regeneration (Demyanenko et al., 2022). However, the molecular mechanism of glutamate-induced excitotoxicity remains elusive. Here, we found that ADSC-EVs exhibited anti-excitotoxic and neuroprotective effects on glutamate-induced retinal damage. Intravitreal injection of ADSC-EVs decreased the intracellular calcium concentration and upregulated surface GluA2 expression, suggesting that ADSC-EVs inhibited the calcium overload by upregulating the GluA2-containing AMPARs. GluA2 phosphorylation is an essential event that decreases the expression of surface GluA2 (Guo and Ma, 2021). Furthermore, GluA2 phosphorylation induced by PKC- $\alpha$  activation was inhibited by ADSC-EVs. These findings support that the regulatory role of ADSC-EVs on the PKC-GluA2 signaling pathway may be an essential mechanism in its anti-excitotoxic effect.

In recent years, matrix-bound nanoparticles, localized in the bioscaffolds of the extracellular matrix, have also been considered as an effective EV-based therapeutic. The extracellular matrix provides the structural basis for cell growth and repair (Swinehart and Badylak, 2016; Mathivanan, 2017), and matrix-bound nanoparticles carry bioactive factors that inhibit inflammatory responses (Huleihel et al., 2017) and promote regeneration (van der Merwe et al., 2017). A recent study found that matrix-bound nanoparticles modulated ischemia-induced RGC injury by intravitreal injection (van der Merwe et al., 2019). Our study indicated that ADSC-EVs regulate the PKC-GluA2 signaling pathway and inhibit retinal excitotoxic injury. Future studies should investigate whether the effectiveness of ADSC-EVs could be improved by modifying extracellular matrix bioscaffolds with ADSC-EVs (Hao et al., 2020a, b).

This study used only male rats in the *in vivo* experiments. Although most previous studies have been performed in male experimental animals (Beery and Zucker, 2011), a recent study reported that testosterone injection can cause open-angle glaucoma and ischemic retinal disease (Dahshan et al., 2022). To avoid bias in the results due to sex and to analyze the damage in the glutamate model and the ADSC-EV therapeutic effects more comprehensively, it is necessary to include female rats in future studies. In addition, only 24 hours were observed after *in vivo* intervention with ADSC-EVs. An extended observation period is needed to further investigate the efficacy and side effects of ADSC-EVs. This study did not investigate which components of ADSC-EVs modulate the PKC-GluA2 pathway, which should be investigated in future studies.

In conclusion, our results indicated that ADSC-EVs ameliorated glutamate-induced retinal damage by inhibiting the phosphorylation of GluA2 and PKC- $\alpha$ . These findings suggest the potential of ADSC-EVs for use in the clinical therapy of retinal diseases.

**Acknowledgments:** We thanked Dr. Kun Xiong (Department of Human Anatomy and Neurobiology, School of Basic Medical Science, Central South University, Changsha, Hunan Province, China) for providing the rat retinal precursor (R28) cells.

**Author contributions:** Experimental design: JFH and DC; experiments implementation: TQD, ZLG and AXL; data collection and analysis: DC, JFH and TQD; manuscript drafting: TQD, JBT and JFH. All authors approved the final version of the manuscript.

**Conflicts of interest:** The authors declare no conflicts of interest.

**Data availability statement:** All data relevant to the study are included in the article and its Additional files.

**Open access statement:** This is an open access journal, and articles are distributed under the terms of the Creative Commons AttributionNonCommercial-ShareAlike 4.0 License, which allows others to remix, tweak, and build upon the work non-commercially, as long as appropriate credit is given and the new creations are licensed under the identical terms.

**Additional file:**

**Additional Figure 1:** Glutamate-induced damage decreased by ADSC-EVs in R28 cells.

## References

- Ahmadian Kia N, Bahrami AR, Ebrahimi M, Matin MM, Neshati Z, Almohaddesin MR, Aghdami N, Bidkhorri HR (2011) Comparative analysis of chemokine receptor's expression in mesenchymal stem cells derived from human bone marrow and adipose tissue. *J Mol Neurosci* 44:178-185.
- Alomar SY, B MB, Eldosoky M, Atef H, Mohamed AS, Elhawary R, El-Shafey M, Youssef AM, Elkazaz AY, Gabr AM, Elaskary AA, Salih MAK, Alolayan SO, Zaitone SA (2021) Protective effect of metformin on rat diabetic retinopathy involves suppression of toll-like receptor 4/nuclear factor-k B expression and glutamate excitotoxicity. *Int Immunopharmacol* 90:107193.
- Bang C, Thum T (2012) Exosomes: new players in cell-cell communication. *Int J Biochem Cell Biol* 44:2060-2064.
- Beery AK, Zucker I (2011) Sex bias in neuroscience and biomedical research. *Neurosci Biobehav Rev* 35:565-572.
- Bowie D, Mayer ML (1995) Inward rectification of both AMPA and kainate subtype glutamate receptors generated by polyamine-mediated ion channel block. *Neuron* 15:453-462.
- Charles-Messance H, Blot G, Couturier A, Vignaud L, Touhami S, Beguier F, Siqueiros L, Forster V, Barro N, Augustin S, Picaud S, Sahel JA, Rendon A, Grosche A, Tadayoni R, Sennlaub F, Guillonnet X (2020) IL-1 $\beta$  induces rod degeneration through the disruption of retinal glutamate homeostasis. *J Neuroinflammation* 17:1.
- Chen TJ, Kukley M (2020) Glutamate receptors and glutamatergic signalling in the peripheral nerves. *Neural Regen Res* 15:438-447.
- Connaughton V (1995) Glutamate and glutamate receptors in the vertebrate retina. In: *Webvision: The Organization of the Retina and Visual System* (Kolb H, Fernandez E, Nelson R, eds). Salt Lake City (UT): University of Utah Health Sciences Center.
- Crowley LC, Marfell BJ, Scott AP, Waterhouse NJ (2016) Quantitation of apoptosis and necrosis by annexin V binding, propidium iodide uptake, and flow cytometry. *Cold Spring Harb Protoc* 2016.

- Cui C, Zang N, Song J, Guo X, He Q, Hu H, Yang M, Wang Y, Yang J, Zou Y, Gao J, Wang L, Wang C, Liu F, He F, Hou X, Chen L (2022) Exosomes derived from mesenchymal stem cells attenuate diabetic kidney disease by inhibiting cell apoptosis and epithelial-to-mesenchymal transition via miR-424-5p. *FASEB J* 36:e22517.
- Cull-Candy SG, Farrant M (2021) Ca<sup>2+</sup>-permeable AMPA receptors and their auxiliary subunits in synaptic plasticity and disease. *J Physiol* 599:2655-2671.
- Dahshan D, Verma V, Goel M (2022) Open-angle glaucoma and ischemic optic neuropathy with injectable testosterone use. *Ophthalmol Glaucoma* 5:244-245.
- Demyanenko SV, Pitinova MA, Kalyuzhnaya YN, Khaitin AM, Batalshchikova SA, Dobaeva NM, Shevtsova YA, Goryunov KV, Plotnikov EY, Pashkevich SG, Sukhikh GT, Silachev DN (2022) Human multipotent mesenchymal stromal cell-derived extracellular vesicles enhance neuroregeneration in a rat model of sciatic nerve crush injury. *Int J Mol Sci* 23:8583.
- Dingledine R, Borges K, Bowie D, Traynelis SF (1999) The glutamate receptor ion channels. *Pharmacol Rev* 51:7-61.
- Dionysopoulou S, Wikström P, Walum E, Thermo K (2020) Effect of NADPH oxidase inhibitors in an experimental retinal model of excitotoxicity. *Exp Eye Res* 200:108232.
- Dominici M, Le Blanc K, Mueller I, Slaper-Cortenbach I, Marini F, Krause D, Deans R, Keating A, Prockop D, Horwitz E (2006) Minimal criteria for defining multipotent mesenchymal stromal cells. The International Society for Cellular Therapy position statement. *Cytotherapy* 8:315-317.
- Dong LD, Gao F, Wang XH, Miao Y, Wang SY, Wu Y, Li F, Wu J, Cheng XL, Sun XH, Yang XL, Wang Z (2015) GluA2 trafficking is involved in apoptosis of retinal ganglion cells induced by activation of EphB/EphrinB reverse signaling in a rat chronic ocular hypertension model. *J Neurosci* 35:5409-5421.
- Dou YQ, Kong P, Li CL, Sun HX, Li WW, Yu Y, Nie L, Zhao LL, Miao SB, Li XK, Dong C, Zhang JW, Liu Y, Huo XX, Chi K, Gao X, Zhang N, Weng L, Yang H, Zhang F, et al. (2020) Smooth muscle SIRT1 reprograms endothelial cells to suppress angiogenesis after ischemia. *Theranostics* 10:1197-1212.
- Fang C, Sun J, Qian J, Shen CL (2023) Oscillating field stimulation promotes neurogenesis of neural stem cells through miR-124/Tal1 axis to repair spinal cord injury in rats. *Neural Regen Res* 18:895-900.
- Guo C, Ma YY (2021) Calcium permeable-AMPA receptors and excitotoxicity in neurological disorders. *Front Neural Circuits* 15:711564.
- Hao D, Ma B, He C, Liu R, Farmer DL, Lam KS, Wang A (2020a) Surface modification of polymeric electrospun scaffolds via a potent and high-affinity integrin  $\alpha 4 \beta 1$  ligand improved the adhesion, spreading and survival of human chorionic villus-derived mesenchymal stem cells: a new insight for fetal tissue engineering. *J Mater Chem B* 8:1649-1659.
- Hao D, Swindell HS, Ramasubramanian L, Liu R, Lam KS, Farmer DL, Wang A (2020b) Extracellular matrix mimicking nanofibrous scaffolds modified with mesenchymal stem cell-derived extracellular vesicles for improved vascularization. *Front Bioeng Biotechnol* 8:633.
- Hao P, Liang Z, Piao H, Ji X, Wang Y, Liu Y, Liu R, Liu J (2014) Conditioned medium of human adipose-derived mesenchymal stem cells mediates protection in neurons following glutamate excitotoxicity by regulating energy metabolism and GAP-43 expression. *Metab Brain Dis* 29:193-205.
- Harrell CR, Volarevic V, Djonov V, Volarevic A (2022) Therapeutic potential of exosomes derived from adipose tissue-sourced mesenchymal stem cells in the treatment of neural and retinal diseases. *Int J Mol Sci* 23:4487.
- Harrell CR, Fellbaum C, Jovicic N, Djonov V, Arsenijevic N, Volarevic V (2019) Molecular mechanisms responsible for therapeutic potential of mesenchymal stem cell-derived secretome. *Cells* 8:467.
- Hartwick AT, Hamilton CM, Baldrige WH (2008) Glutamatergic calcium dynamics and deregulation of rat retinal ganglion cells. *J Physiol* 586:3425-3446.
- Hearner R, Sandhar B, Vyas V, Longhi MP (2021) Isolation of stromal vascular fraction cell suspensions from mouse and human adipose tissues for downstream applications. *STAR Protoc* 2:100422.
- Huang Y, Wang S, Huang F, Zhang Q, Qin B, Liao L, Wang M, Wan H, Yan W, Chen D, Liu F, Jiang B, Ji D, Xia X, Huang J, Xiong K (2021) c-FLIP regulates pyroptosis in retinal neurons following oxygen-glucose deprivation/recovery via a GSDMD-mediated pathway. *Ann Anat* 235:151672.
- Huleihel L, Bartolacci JG, Dziki JL, Vorobyov T, Arnold B, Scarritt ME, Pineda Molina C, LoPresti ST, Brown BN, Naranjo JD, Badylak SF (2017) Matrix-bound nanovesicles recapitulate extracellular matrix effects on macrophage phenotype. *Tissue Eng Part A* 23:1283-1294.
- Jacobi E, von Engelhardt J (2017) Diversity in AMPA receptor complexes in the brain. *Curr Opin Neurobiol* 45:32-38.
- Kou ZW, Mo JL, Wu KW, Qiu MH, Huang YL, Tao F, Lei Y, Lv LL, Sun FY (2019) Vascular endothelial growth factor increases the function of calcium-impermeable AMPA receptor GluA2 subunit in astrocytes via activation of protein kinase C signaling pathway. *Glia* 67:1344-1358.
- Kuns B, Rosani A, Varghese D (2022) Memantine. In: *StatPearls*. Treasure Island (FL): StatPearls Publishing.
- Lee JU, Park KJ, Kim KH, Choi MK, Lee YH, Kim DH (2020) What is the ideal entry point for transforaminal endoscopic lumbar discectomy? *J Korean Neurosurg Soc* 63:614-622.
- Liu Z, Qiu X, Ma S, Guo B, Hu S, Wang J, Luo F, Xu D, Sun Y, Zhang G, Cui G, Wang Y, Zhang Z, Han Y (2020) Multifunctional memantine nitrate significantly protects against glutamate-induced excitotoxicity via inhibiting calcium influx and attenuating PI3K/Akt/GSK3beta pathway. *Chem Biol Interact* 325:109020.
- Mathew B, Ravindran S, Liu X, Torres L, Chennakesavalu M, Huang CC, Feng L, Zelka R, Lopez J, Sharma M, Roth S (2019) Mesenchymal stem cell-derived extracellular vesicles and retinal ischemia-reperfusion. *Biomaterials* 197:146-160.
- Mathivanan S (2017) Extracellular matrix and the extracellular environment. *Proteomics* 17:7700185.
- McCulloch DL, Marmor MF, Brigell MG, Hamilton R, Holder GE, Tzekov R, Bach M (2015) ISCEV Standard for full-field clinical electroretinography (2015 update). *Doc Ophthalmol* 130:1-12.
- Papazian I, Kyrargyri V, Evangelidou M, Voulgari-Kokota A, Probert L (2018) Mesenchymal stem cell protection of neurons against glutamate excitotoxicity involves reduction of NMDA-triggered calcium responses and surface GluR1, and is partly mediated by TNF. *Int J Mol Sci* 19:651.
- Percie du Sert N, Hurst V, Ahluwalia A, Alam S, Avey MT, Baker M, Browne WJ, Clark A, Cuthill IC, Dirnagl U, Emerson M, Garner P, Holgate ST, Howells DW, Karp NA, Lazic SE, Lidster K, MacCallum CJ, Macleod M, Pearl EJ, et al. (2020) The ARRIVE guidelines 2.0: Updated guidelines for reporting animal research. *PLoS Biol* 18:e3000410.
- Phinney DG, Pittenger MF (2017) Concise review: MSC-derived exosomes for cell-free therapy. *Stem Cells* 35:851-858.
- Purkey AM, Dell'Acqua ML (2020) Phosphorylation-dependent regulation of Ca<sup>2+</sup>-permeable AMPA receptors during hippocampal synaptic plasticity. *Front Synaptic Neurosci* 12:8.
- Schneider CA, Rasband WS, Eliceiri KW (2012) NIH image to ImageJ: 25 years of image analysis. *Nat Methods* 9:671-675.
- Sisk DR, Kuwabara T (1985) Histologic changes in the inner retina of albino rats following intravitreal injection of monosodium L-glutamate. *Graefes Arch Clin Exp Ophthalmol* 23:250-258.
- Swinehart IT, Badylak SF (2016) Extracellular matrix bioscaffolds in tissue remodeling and morphogenesis. *Dev Dyn* 245:351-360.
- van der Merwe Y, Faust AE, Steketee MB (2017) Matrix bound vesicles and miRNA cargoes are bioactive factors within extracellular matrix bioscaffolds. *Neural Regen Res* 12:1597-1599.
- van der Merwe Y, Faust AE, Sakalli ET, Westrick CC, Hussey G, Chan KC, Conner IP, Fu VLN, Badylak SF, Steketee MB (2019) Matrix-bound nanovesicles prevent ischemia-induced retinal ganglion cell axon degeneration and death and preserve visual function. *Sci Rep* 9:3482.
- Vernazza S, Oddone F, Tirendi S, Bassi AM (2021) Risk factors for retinal ganglion cell distress in glaucoma and neuroprotective potential intervention. *Int J Mol Sci* 22:7994.
- Wang S, Liao L, Huang Y, Wang M, Zhou H, Chen D, Liu F, Ji D, Xia X, Jiang B, Huang J, Xiong K (2019) Pin1 is regulated by CaMKII activation in glutamate-induced retinal neuronal regulated necrosis. *Front Cell Neurosci* 13:276.
- Wasilewa P, Hockwin O, Korte I (1976) Glycogen concentration changes in retina, vitreous body and other eye tissues caused by disturbances of blood circulation. *Albrecht Von Graefes Arch Klin Exp Ophthalmol* 199:115-120.
- Xin D, Li T, Chu X, Ke H, Yu Z, Cao L, Bai X, Liu D, Wang Z (2020) Mesenchymal stromal cell-derived extracellular vesicles modulate microglia/macrophage polarization and protect the brain against hypoxia-ischemic injury in neonatal mice by targeting delivery of miR-21a-5p. *Acta Biomater* 113:597-613.
- Xu LX, Tang XJ, Yang YY, Li M, Jin MF, Miao P, Ding X, Wang Y, Li YH, Sun B, Feng X (2017) Neuroprotective effects of autophagy inhibition on hippocampal glutamate receptor subunits after hypoxia-ischemia-induced brain damage in newborn rats. *Neural Regen Res* 12:417-424.
- Yan WT, Zhao WJ, Hu XM, Ban XX, Ning WY, Wan H, Zhang Q, Xiong K (2023) PANoptosis-like cell death in ischemia/reperfusion injury of retinal neurons. *Neural Regen Res* 18:357-363.
- Yang D, Zhang W, Zhang H, Zhang F, Chen L, Ma L, Larcher LM, Chen S, Liu N, Zhao Q, Tran PHL, Chen C, Veedu RN, Wang T (2020) Progress, opportunity, and perspective on exosome isolation - efforts for efficient exosome-based theranostics. *Theranostics* 10:3684-3707.
- Yao F, Peng J, Zhang E, Ji D, Gao Z, Tang Y, Yao X, Xia X (2022) Pathologically high intraocular pressure disturbs normal iron homeostasis and leads to retinal ganglion cell ferroptosis in glaucoma. *Cell Death Differ* doi: 10.1038/s41418-022-01046-4.
- Yu B, Li XR, Zhang XM (2020) Mesenchymal stem cell-derived extracellular vesicles as a new therapeutic strategy for ocular diseases. *World J Stem Cells* 12:178-187.
- Zaitone SA, Alshaman R, Alattar A, Elsherbiny NM, Abogresha NM, El-Kherbetawy MK, Elaskary AA, Hashish AA, Rashed LA, Ahmed E (2020) Retinoprotective effect of donepezil in diabetic mice involves mitigation of excitotoxicity and activation of PI3K/mTOR/BC(2) pathway. *Life Sci* 262:118467.
- Zhang C, Huang Y, Ouyang F, Su M, Li W, Chen J, Xiao H, Zhou X, Liu B (2022) Extracellular vesicles derived from mesenchymal stem cells alleviate neuroinflammation and mechanical allodynia in interstitial cystitis rats by inhibiting NLRP3 inflammasome activation. *J Neuroinflammation* 19:80.
- Zhao L, Wei X, Ma Z, Feng D, Tu P, Johnstone BH, March KL, Du Y (2009) Adipose stromal cells-conditional medium protected glutamate-induced CGNs neuronal death by BDNF. *Neurosci Lett* 452:238-240.
- Zhuang Z, Liu M, Luo J, Zhang X, Dai Z, Zhang B, Chen H, Xue J, He M, Xu H, Liu A (2022) Exosomes derived from bone marrow mesenchymal stem cells attenuate neurological damage in traumatic brain injury by alleviating glutamate-mediated excitotoxicity. *Exp Neurol* 357:114182.

C-Editor: Zhao M; S-Editors: Yu J, Li CH; L-Editors: McCollum L, Yu J, Song LP; T-Editor: Jia Y